JMEPEG (2020) 29:5273–5281
https://doi.org/10.1007/s11665-020-05047-7

1059-9495/$19.00

Microstructures and Mechanical Properties of As-Extruded AZ31−*x*Sm Magnesium Alloy

Ming Sun, Meijuan Liu, Binghui Zhang, Zezhong Chen, and Hong Jiang

(Submitted December 20, 2019; in revised form May 21, 2020; published online August 19, 2020)

The effects of Samarium (Sm) on the microstructures and mechanical properties of as-extruded AZ31 Mg alloy have been investigated. It is shown that the grain size changes in a non-monotonic mode of firstly coarsening and then refining, where the alloys with 0 ∼ 1.18wt.%Sm have bimodal grain structure consisted of dynamic recrystallized (DRXed) grains and unDRXed grains, while the alloys with 2.17 ∼ 3.13wt.%Sm have fully DRXed fine grains. A fine as-cast microstructure produces a finer extruded microstructure, and a large amount of tiny $Al_{11}Sm_3$ particle is necessary to generate DRXed grains through particle-stimulated nucleation (PSN) effect. However, bigger Al_2Sm particles can lead to increase in both area fraction of larger grains (above 40 µm) and texture, due to less effective in both PSN effect and suppressing DRXed grain growth. Grain refinement, secondary phase distribution and texture are important factors determining the mechanical properties of extruded alloys. Due to the fine grains, large amount of tiny secondary phase and suitable texture intensity, alloy with 3.13%Sm has the best mechanical property (i.e., YS 198 MPa, UTS 272 MPa and elongation 10%).

Keywords AZ31, extrusion, magnesium alloy, mechanical property, microstructure

1. Introduction

Mg alloys show great application potentials in automobile and aerospace industries due to lower density and higher specific strength than aluminum alloys and iron materials (Ref 1). AZ31 (Mg-3Al-1Zn-0.3Mn, in wt.%) alloy is one kind of low-cost Mg-Al alloy, which is normally used as wrought alloy that can be produced by plastic forming (Ref 2). During hot deformation, a fine grain size of ingot before plastic forming is important for the subsequent mechanical properties. However, one major issue of Mg-Al alloy is that grain refinement during casting is still difficult, although various approaches have been trialed over the last decades, such as solute element addition, superheating, Elfinal and carbon inoculation (Ref 3-5).

Recently, rare earth (RE) elements have been reported to exhibit grain refinement effect on Mg alloys through the formation of heterogeneous nucleating particles Al_2Y (Ref 6, 7), Al_2Gd (Ref 8) or Al_2Sm (Ref 9-12). Due to grain refinement by Al_2Sm and suppression of micro-galvanic corrosion by Al-Sm-Mn compounds (Ref 13, 14), the corrosion resistance of AZ31 alloy can be significantly improved by 1.5% Sm addition. Additionally, Sm is a much cheaper RE element compared with Y and Gd. Therefore, Sm is thought to be a good choice of alloying element for development of new Mg alloys.

Ming Sun, Meijuan Liu, Binghui Zhang, Zezhong Chen, and **Hong Jiang**, School of Materials Science and Engineering, University of Shanghai for Science and Technology, Shanghai 200093, People's Republic of China. Contact e-mail: zzhchen@usst.edu.cn.

Latest work (Ref 9, 10) has investigated the effect of Sm on grain refinement of as-cast AZ31 alloy. An interesting finding is that the grain size can be coarsened or refined. When Sm content is far below 2 wt.%, for example, 0.2%, serious grain coarsening occurs. The coarsening effect is because the addition of Sm reduces the constitutional supercooling refinement effect (Ref 9) and possibly removes or poisons the "native" Al-Fe-C-O nucleating particles in Mg melt (Ref 10). On the contrary, when Sm content is above 2 wt.%, Al_2Sm nucleating particles can be in situ formed, and thus, excellent grain refinement can be obtained (Ref 9, 10). However, the detailed effects of Sm on microstructure and mechanical properties of AZ31 alloy during plastic deformation are still not very clear. Therefore, this study investigates the microstructure and mechanical properties of extruded AZ31−*x*Sm alloys, which is helpful to the development of new Mg alloys.

2. Experimental Procedure

2.1 Casting Experiments

The alloy ingots in the present study are same with those in our previous study (Ref 9), and they were subjected to extrusion. The casting process will not be repeated in details here. It is briefly mentioned that AZ31−*x*Sm (nominal $x = 0 \sim 3$ wt.%) alloys were melt from raw materials of pure Mg (99.8 wt.%), pure Al (99.85 wt.%), pure Zn (99.99 wt.%) and master alloys Al-10%Mn and Mg-30%Sm in an electric resistance furnace (SG2-3-10). The protective gas is consisted of 99.5vol.%CO_2 and 0.5vol.%SF_6. The real compositions listed in Table 1 were determined by ICP-AES method at Shanghai University, China.

2.2 Extrusion Experiments

The present study focuses on the subsequent hot extrusion of these alloys. The as-cast billets were solution-treated at

410 °C for 20 h followed by water quenching. Then, the solution-treated billets were machined into cylinders with Ø37.5 mm × h50 mm (diameter × height) for extrusion. The extrusion experiments were conducted with a YA32-3150KN hydraulic press at Shanghai Jiao Tong University as shown in Fig. 1(a). The extrusion parameters were as follows: the billet and mold being preheated at ~ 350 °C for ~ 1 h, extrusion ratio 9 (i.e., final size Ø12.5 mm as shown in Fig. 1b) and extrusion rate 2 mm/s. After extrusion, the alloy bars directly fell into the bucket filled with water that located under the machine to ensure quick water quenching.

2.3 Characterization Experiments

The experiments of microstructure observation and tensile testing were same with those in our previous study (Ref 9). For microstructure observations, the specimens were prepared through standard metallographic procedures including grounding, polishing and etching (etchant of acetic-picral solution: 4.2 g picric acid, 10 ml acetic acid, 80 ml ethyl alcohol and 10 ml water). The microstructure was observed on optical microscopy (Zeiss A1) and scanning electron microscope (FEI Nova NanoSEM 230) equipped with detectors energy-dispersive spectrum (EDS), backscatter electron (BSE) and electron back-scattering diffraction (EBSD). EBSD data were analyzed using the Oxford Channel 5 software to obtain the inverse pole figure (IPF) maps, recrystallized maps and so on. During EBSD scanning, ED, TD and ND meant extrusion direction, tangential direction and normal direction, respectively.

For tensile property tests, the flat specimens as shown in Fig. 2 were cut from the extruded bars along the extrusion direction (ED) by electric-spark wire-cutting. The gage dimensions of the specimens were 48 × 18 × 1.5 mm^3. The tensile testing was conducted on a Zwick/Roell-20KN material test machine at a cross-head speed of 0.5 mm/min at room temperature. For each alloy, seven parallel specimens were tested in order to calculate average values for yield strength (YS, MPa), ultimate tensile strength (UTS, MPa) and elongation to failure (%).

Table 1 The chemical compositions (wt.%) determined by ICP-AES

Alloy	Al	Zn	Mn	Sm	Fe
0Sm	2.76	0.84	0.28	…	0.023
0.3Sm	2.85	0.91	0.29	0.32	0.023
1Sm	2.86	0.93	0.28	1.18	0.035
2Sm	2.76	0.87	0.26	2.17	0.012
3Sm	3.02	0.97	0.27	3.13	0.035

Same ingots with our previous study (Ref 9)

3. Results and Discussion

3.1 Phase and Grain Size of As-Cast Alloys

The phases and grain size of as-cast counterparts (i.e., initial ingots) have already been reported in our previous work (Ref 9). This information is only simply described for analysis.

(i) The main phases of base alloy AZ31 are composed of α-Mg matrix and β-$Mg_{17}(Al, Zn)_{12}$. The function of Zn and Mn in Mg-Al-Zn-Mn series alloy is to improve the alloy castability (especially fluidity) and corrosion resistance, respectively. Zn segregates to $Mg_{17}Al_{12}$ forming ternary β-$Mg_{17}(Al, Zn)_{12}$ phase. However, β-phase can always be written as β-$Mg_{17}Al_{12}$ in most of the researches on Mg-Al-Zn alloys. Mn forms Al_6MnFe_x phase that prevents the formation of Al_3Fe phase that is harmful to corrosion resistance, while excessive Mn forms Al_8Mn_5 phase. Al_8Mn_5 phase could not be detected by XRD due to the low content of Mn (0.3 wt.%). After Sm was added, the β-$Mg_{17}Al_{12}$ secondary phase was gradually replaced by new phases of needle-like (or strip-like) $Al_{11}Sm_3$ and polygonal-shaped Al_2Sm (Ref 9-12) due to the preferential reactions be-

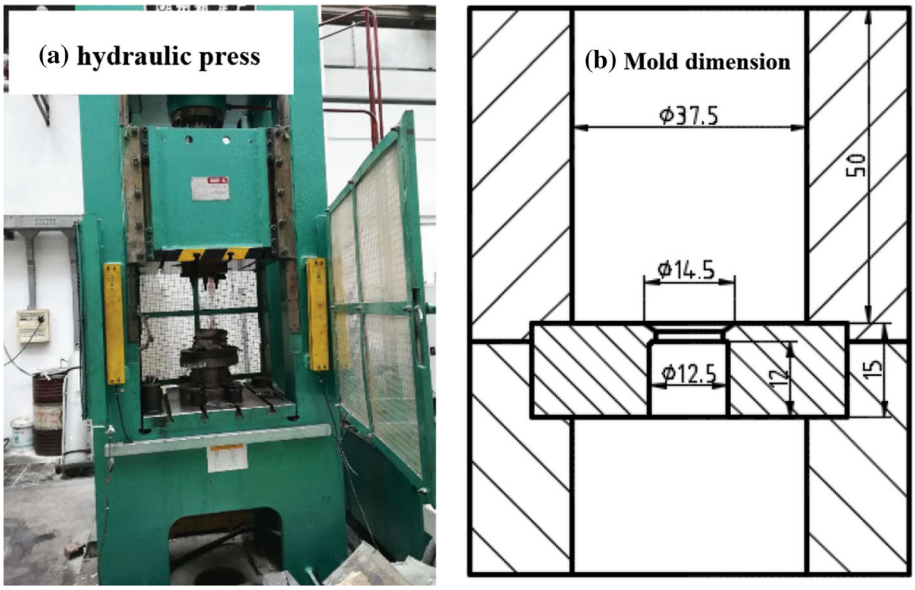

Fig. 1 (a) Photograph of the YA32-3150KN hydraulic press, and (b) schematic diagram of molds for hot extrusion (extrusion ratio 9)

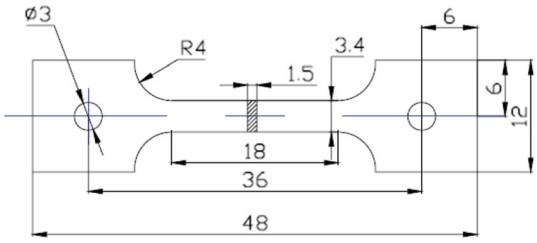

Fig. 2 Dimension of tensile test sample (Reproduced from (Ref 9)). Tensile direction is parallel to extrusion direction (ED)

tween Al and Sm. In addition, the volume fraction (vol.%) of secondary phase in the five as-cast alloys was 1.2%, 1.4%, 4.4%, 5.1% and 8.8%, respectively (data from Ref 9).

(ii) The grain size of AZ31 with Sm content of 0, 0.32, 1.18, 2.17 and 3.13 wt.% was 462 ± 22 μm, 1519 ± 114 μm, 1075 ± 55 μm, 357 ± 20 μm and 173 ± 6 μm, respectively (data from Ref 9). The grain morphology changed from dendrite to fully equiaxed grains at 3.13% Sm alloy. It showed a non-monotonic tendency of "initial coarsening and subsequent refinement," which was in good agreement with Ref (10, 12). Grain coarsening effect was attributed to the reactions between Al and Sm which reduced constitutional supercooling effect on grain refinement, and the addition of Sm probably poisoned the native Al-Fe-C-O nucleating particles (Ref 9, 10, 12). In contrast, grain refinement effect was because of the in situ formation of Al_2Sm particles, whose heterogeneous nucleation potency was powerful due to a low lattice misfit with Mg (only 0.45%, Ref 13). Moreover, the large amount of needle-like Al11Sm3 phase also restrained dendrites or grains from growing.

3.2 Microstructure of As-Extruded Alloys

Before SEM and EBSD observations, the qualitative observations through optical microscope were firstly conducted for initial analysis. Figure 3 shows the optical microstructure of the plane ED–TD (ED: extrusion direction, TD: tangential direction) of as-extruded alloys. It can be seen that the extruded alloys have extrusion streamlines along the ED, which is the typical feature of extruded alloys. The qualitative observation of grain morphologies exhibits two points as follows, which will be explained later with quantitative analysis of EBSD data in Fig. 5.

(i) The DRXed grain size was firstly coarsened and then refined, where the critical value of Sm content was 0.32%. Moreover, a minor detail could also be seen that the grain size of 2.17%Sm alloy seemed to be slightly increased again.

(ii) The grain structure was not constant for all alloys. The first three as-extruded alloys (with $0 \sim 1.18$ wt.%Sm) exhibited a bimodal grain structure consisting of DRXed fine grains and unDRXed grains, while the latter two alloys (with 2.17% and 3.13%Sm) had fully DRXed grain structure. When Sm content was increased from 0 to 0.32%, the unDRXed region was obviously increased. However, when Sm content was further increased, the unDRXed region was rapidly decreased. This was mainly due to the increase in particle-stimulated nucleation (PSN) effect, which will be discussed later after the EBSD data.

Figure 4 shows the typical SEM microstructures and EDS results. It should be firstly mentioned that the EDS acquisition of $Al_{11}Sm_3$ phase could not be well conducted due to its very tiny size ($1 \sim 3$ μm) after extrusion, while its original morphology and EDS compositions in as-cast alloys can be referred to Ref (9). Two points can be seen from Fig. 4. One point is that the amount of secondary phase from Fig. 4(a) to (d) in as-extruded alloys was gradually increased, which was in good agreement with as-cast counterparts. Another point is that the fragment extent between $Al_{11}Sm_3$ and Al_2Sm particles was different during extrusion. The needle-like $Al_{11}Sm_3$ particles presented in as-cast alloys were effectively crushed into smaller ones (mostly $1 \sim 3$ μm) distributing along the streamlines due to the strong deformation force. But most of the Al_2Sm particles were not fragmented as shown in Fig. 4(d), (d′) and (f). This judgment was based on the comparisons of particle shape and size between as-cast and as-extruded alloys. It is obvious that the un-fragmented Al_2Sm particles still had the polygonal shape with $5 \sim 9$ μm size, similar to the original ones in as-cast alloys (Ref 9). Therefore, the two points regarding distribution of secondary phase would influence the DRX behavior and final mechanical properties, which will be discussed later. In addition, the sphere-like Al_8Mn_5 particles with about 4 μm diameter were occasionally found in the as-extruded alloys as shown in Fig. 4(b′) and (e). The presence of small proportion of Sm element in Fig. 4(e′) was due to the segregation of Sm to Al_8Mn_5 phase, which formed Al-Mn-Sm phase (Ref 15). Due to negligible number, the Al_8Mn_5 or Al-Mn-Sm particles will be neglected during the following analysis of DRX behavior.

3.3 EBSD Analysis of As-Extruded Alloys

Figure 5 shows the EBSD inverse pole figures (IPF) and texture images of as-extruded alloys, where the scanning direction is parallel to the ED (i.e., the observation plane same with Fig. 3 and 4). Figure 6(a) further shows the grain size distribution obtained from EBSD analysis, and Fig. 6(b) further plots the "total area fraction of coarse grains larger than a critical size (40 μm as marked in Fig. 6a)." The evolutions in grain and texture were analyzed, respectively, in the following paragraphs. It is additionally mentioned that although the Mg-Al-Sm alloy is quite similar to that studied by Fu et al. (Ref 12), the extruded grain size is greatly larger than their value. In this study, the size of equiaxed grain and long grain is within the range of $8 \sim 40$ μm and $40 \sim 170$ μm, respectively. However, the size of most grains is within the range of $6 \sim 12$ μm in Ref 12. This could be due to the differences in extrusion ratio, i.e., 9 in the present study compared with 17.4 by Ref (12).

(i) As mentioned in Fig. 3, the first three alloys had a bimodal grain structure, while the latter two alloys had equiaxed grains structure; the grain size showed coarsening or refinement effects. EBSD results in Fig. 5 further confirmed this, i.e., the grain structure was not constant, and grain size changed in a non-monotonic way. The reasons for the evolutions in grain structure and grain size lie in two important aspects. The first aspect was due to the microstructure heredity, i.e., coarse as-cast microstructure normally leads to coarse

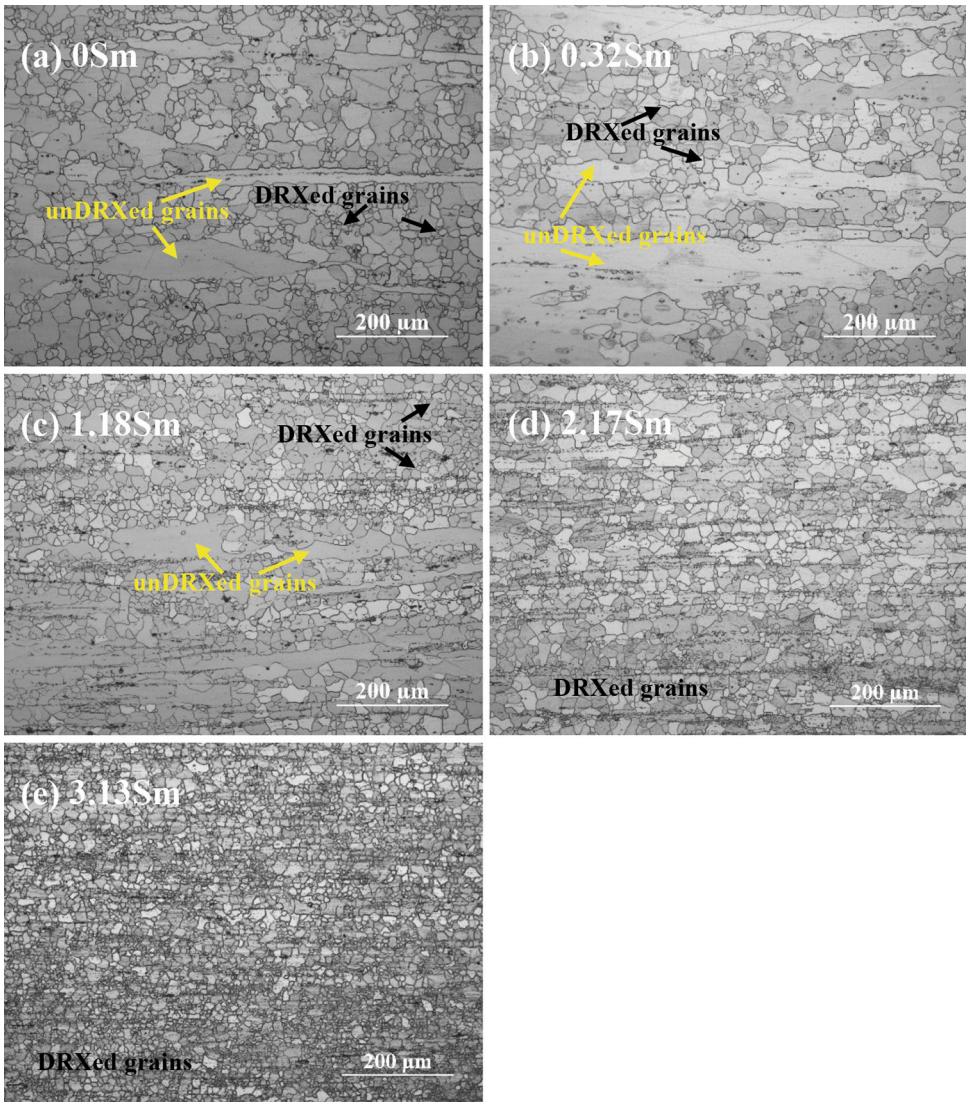

Fig. 3 The optical microstructures of as-extruded AZ31−*x*Sm alloys, where *x* is (a) 0; (b) 0.32%; (c) 1.18%; (d) 2.17%; and (e) 3.13%, respectively

deformed microstructure. However, the second aspect due to the particle-stimulated nucleation (PSN) effect during plastic deformation (Ref 12, 16-18) is much more important. PSN mechanism indicates rapid sub-boundary migration in the deformation zone that necessarily forms around large hard particles during deformation, leading to the creation of new high-angle grain boundaries (HAGBs) (Ref 16). The dispersed fine intermetallic particles generate local inhomogeneity of the strain energy and enhance driving force of recrystallization and finally promote the grain nucleation rate (Ref 12, 16). Moreover, the finely distributed particles can also pin up grain boundaries and then suppress the moving or growth of DRXed grains according to Zener effect (Ref 12, 17, 18). Based on these theories, the changes in grain structure and grain size of as-extruded alloys can be explained.

When Sm content was 0 or 0.32%, the alloys had very coarse grain size of 462 ± 22 μm and 1519 ± 114 μm as shown in Sect. 3.1 (data from Ref 9), respectively. During extrusion process, the coarse grains could not be fully DRXed and lead to a bimodal grain structure, because PSN effect was not so strong due to a low amount of secondary phase particles (i.e., 1.2 vol.% or 1.4 vol.%) in as-cast 0 or 0.32% Sm alloy. Thus, the microstructure heredity resulted in coarse grain in the as-extruded 0Sm or 0.32%Sm alloy.

When Sm content was further increased from 0.32% to 1.18%, the as-cast grain size was refined from 1519 ± 114 μm to 1075 ± 55 μm. Although the grain size was still at a coarser level than the base alloy (462 ± 22 μm), DRXed grains could be obtained due to PSN mechanism since the amount of secondary phase particles was greatly increased to 4.4 vol.%.

When Sm content was continuously increased to 2.17%, the as-cast grain size was obviously refined to 357 ± 20 μm, and the amount of secondary phase particles was further increased to 5.1 vol.%. According to the above theories, both factors including microstructure heredity and PSN effect resulted in the fully DRXed grain structure in 2.17% Sm alloy. However, the area fraction of grains larger than 40 μm was increased from 15.3 vol.% to 25.7 vol.% as clearly shown in Fig. 6(b). This result meant the grain size increased to some extent, which was similar to the extruded AZ31-0.3La-1.0Sm alloy reported by Fu et al. (Ref 12). This could probably be attributed to the presence of large Al_2Sm particles with a local aggregation distribution as

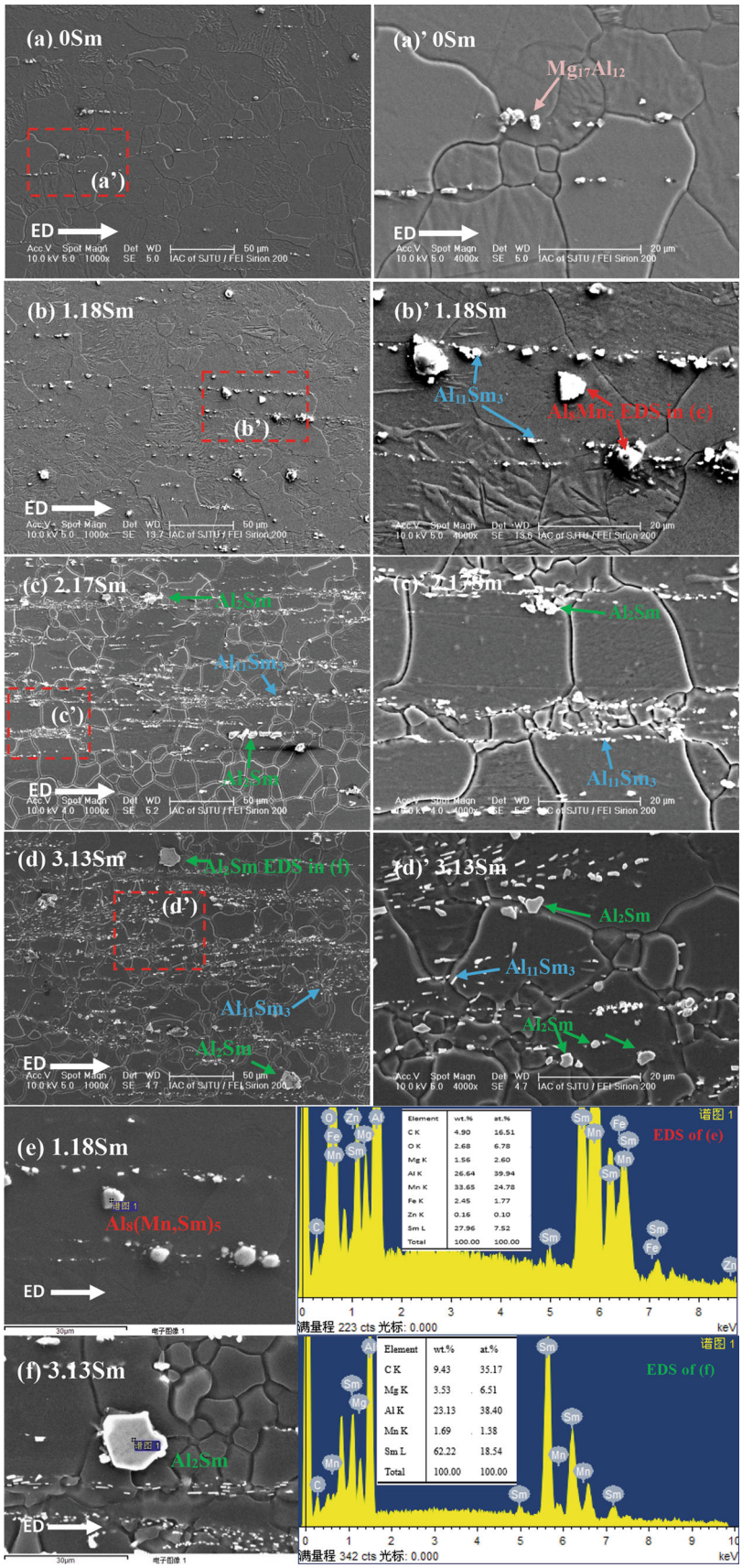

Fig. 4 SEM microstructures of as-extruded AZ31−*x*Sm alloy: (a) ∼ (a′) 0Sm; (b) ∼ (b′) 1.18Sm; (c) ∼ (c′) 2.17Sm; (d) ∼ (d′) 3.13Sm; and (e) ∼ (f) EDS results of particle marked in (b′) and (d)

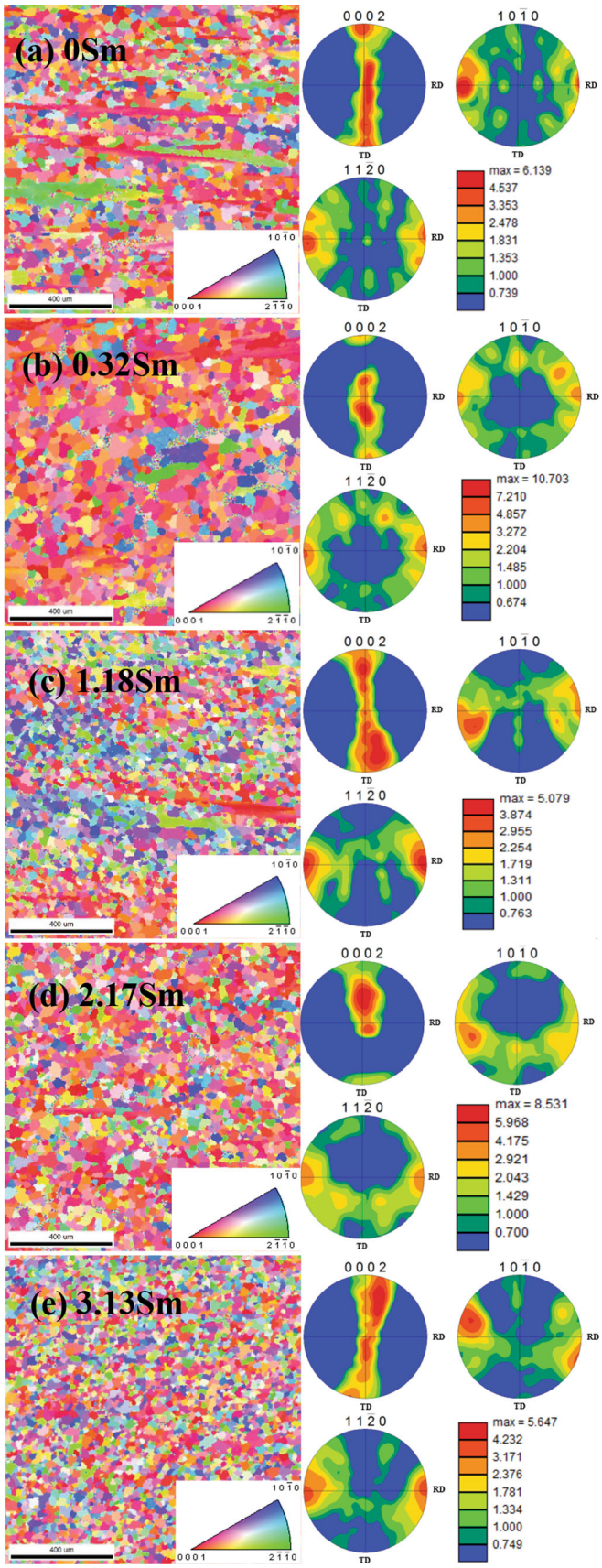

Fig. 5 EBSD analysis showing IPF (left column) and texture (right column) of extruded alloys with: (a) 0Sm; (b) 0.32%Sm; (c) 1.18%Sm; (d) 2.17%Sm; and (e) 3.13%Sm. Grain size distributions are further plotted in Fig. 6

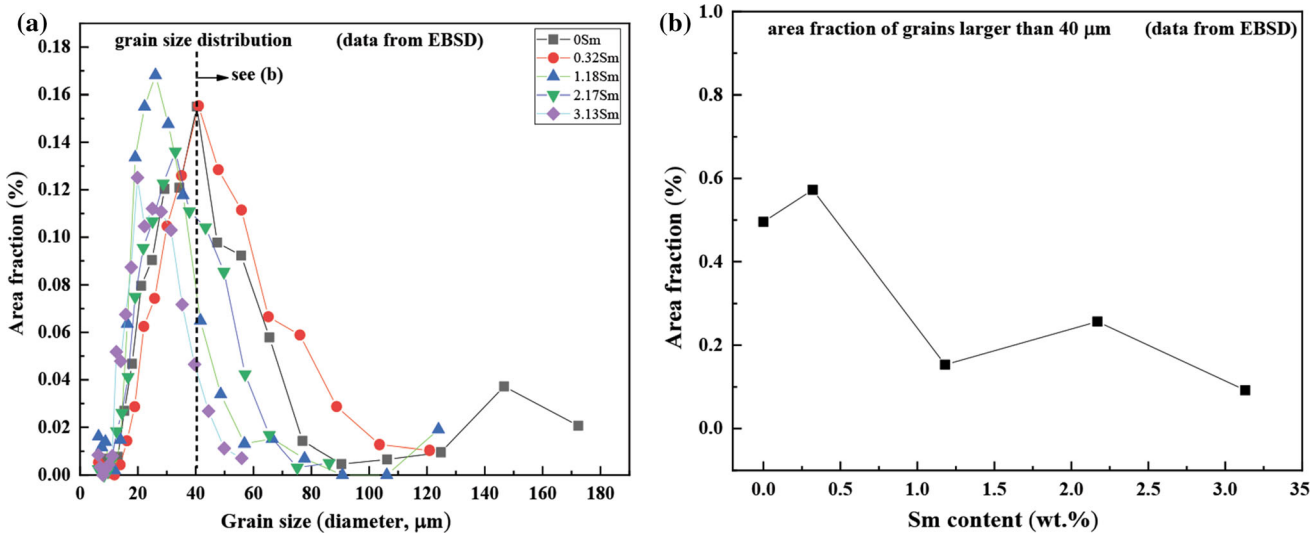

Fig. 6 Grain size distributions obtained from Fig. 5 EBSD data showing: (a) grain size diameter distribution; (b) area fraction of grains larger than 40 μm

shown in Fig. 4(c) and (c′). It has been accepted that when the particle size is too large, the strain accumulation of α-Mg matrix and driving force for RDX will be smaller, which reduces PSN effect (Ref 12). Moreover, large particle is less effective in suppressing grain growth during DRX process (Ref 12).

When Sm content was continuously increased to 3.13%, the as-cast grain size was remarkably refined to 173 ± 6 μm by the Al_2Sm nuclei, and the amount of secondary phase particles was dramatically increased to 8.8vol.%. Both the microstructure heredity and PSN effects lead to the fully DRXed grains with size much finer than the rest four alloys.

In a word, the unDRXed region was gradually reduced with increasing Sm content from 0 to 3.13%. The most important reason was attributed to the PSN effect.

(ii) All the five alloys had obvious (0001) basal texture but with different texture intensities. Grain size, solid solution atoms and secondary phase particles aggregating at grain boundaries influence the PSN effect and then the texture (Ref 12). Robson et al. (Ref 16) reported that texture of DRXed grains via particle-stimulated nucleation (PSN) appeared to be more random. That is to say, the evolutions in texture intensity in Fig. 5 could be mostly related to the distribution of DRXed or unDRXed regions. For example, when Sm content was increased from 0 to 0.32%, the unDRXed region was increased, which leads to a higher texture intensity. When Sm content was increased from 0.32 to 1.1.8%, the unDRXed region was decreased, which leads to a lower texture intensity. However, when Sm content was increased from 1.18 to 2.17%, the texture was increased. This was because the bigger Al_2Sm particles were less effective in PSN effect and suppressing grain growth, which resulted in an increased unDRXed region and then a higher texture intensity. When Sm content was increased from 2.17 to 3.13%, the DRXed grains were dominant, which decreased texture intensity.

3.4 Tensile Properties of As-Extruded Alloys

Figure 7 shows the tensile properties of as-extruded AZ31−*x*Sm alloys. It can be seen that the change in ultimate tensile strength was very slight (all UTS at about 268 MPa).

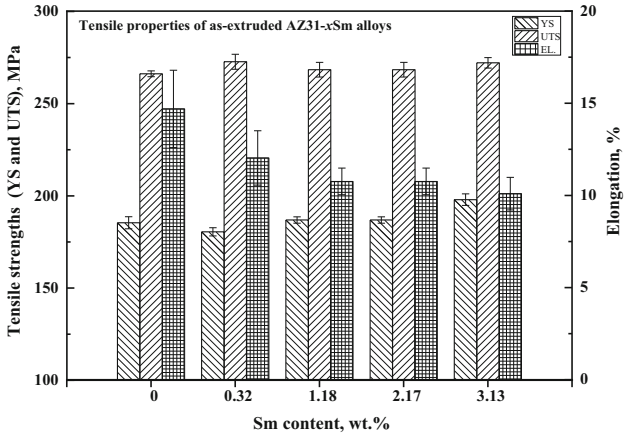

Fig. 7 Room temperature tensile properties of as-extruded AZ31−*x*Sm alloys

The yield strength (YS) first decreased when Sm content was increased from 0 to 0.32 wt.% and then increased when Sm content was about 1.18 ∼ 3.13 wt.%. The elongation decreased linearly, i.e., from ∼ 15 ± 2% to ∼ 10 ± 1%. The best mechanical property was obtained at 3.13% Sm, i.e., YS 198 ± 3 MPa, UTS 272 ± 3 MPa and elongation 10%. Generally, the strengthening factors for mechanical property of alloy include grain refinement, solid solution, aging precipitates, secondary phase and textures. These factors will be discussed as follows.

(i) Solid solution strengthening. As can be seen from the binary phase diagrams of Mg-Al and Mg-Zn (Ref 19), the maximum solubility of Al and Zn in Mg is 12.7 wt.% at 437 °C and 6.2 wt.% at 340 °C, respectively; the solubility of Al and Zn in Mg decreases to below 2 wt.% at room temperature. Thus, before Sm was added in AZ31 alloy, Al and Zn elements had certain degree of solid solution strengthening effect. However, after Sm was added, the reactions between Sm an Al (i.e., forming Al_2Sm or $Al_{11}Sm_3$ precipitates) reduced

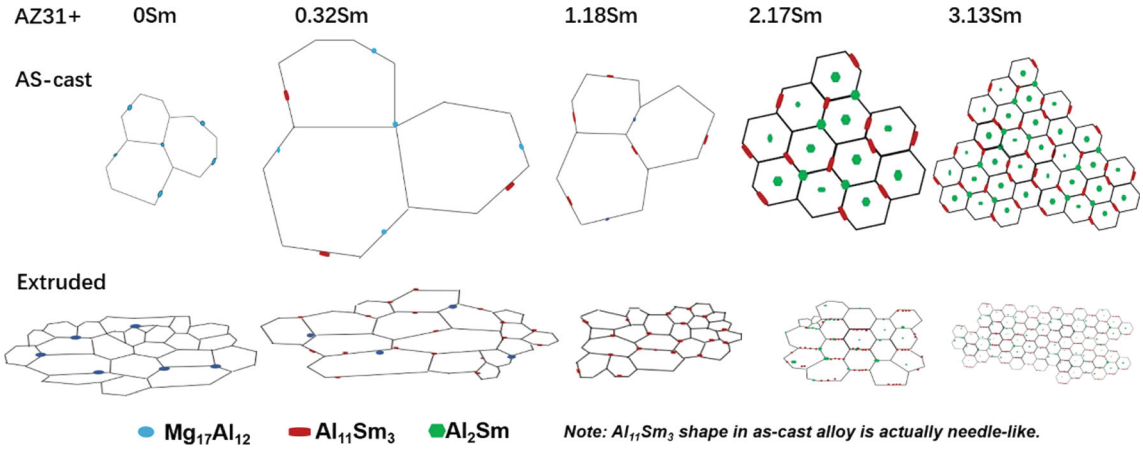

Fig. 8 Schematic illustration showing microstructure evolution of AZ31−*x*Sm alloys under as-cast and as-extruded conditions

the solid solution effect. The content of Zn is only 1 wt.%, which has very slight solid solution strengthening effect. Therefore, solid solution strengthening is negligible for Sm-bearing AZ31 alloys.

(ii) Dynamic precipitate strengthening. When Al content is as high as 9 wt.%, AZ91 alloy exhibits stronger aging precipitate behavior. Kim et al. showed that dynamic precipitates of $Mg_{17}Al_{12}$ can form during hot extrusion process of AZ91 alloy, which can greatly influence the mechanical properties (Ref 20). In the present study, dynamic precipitate mainly formed in base alloy AZ31 due to a solution-treated state before extrusion. However, the dynamic precipitate effect in Sm-bearing alloys is very weak, because the Al solute mainly existed in $Al_{11}Sm_3$ and Al_2Sm phases which could not be dissolved into Mg matrix due to high thermal stability during solution treatment before extrusion.

(iii) Grain refinement strengthening. Figure 5 and 6 shows that the changes in grain size of AZ31−*x*Sm alloy were in a non-monotonic mode including firstly grain coarsening and then grain refinement. Figure 6 shows that the yield strength firstly decreased and then increased. Therefore, yield strength and grain size of AZ31−*x*Sm alloy exhibited the same evolution feature, which fitted well with the Hall–Petch rule (Ref 21).

(iv) Secondary phase strengthening. As shown in Sect. 3.1, the volume fraction of secondary phase in as-cast alloy continued to increase from 1.2vol.% to 8.8vol.%. During subsequent hot extrusion process, the needle-like $Al_{11}Sm_3$ particles were crushed into tiny ones, which could hinder the slip of dislocation during tensile test and exhibited secondary phase strengthening effect. Therefore, the alloys with 3.13% Sm had the highest yield strength of 198 ± 3 MPa due to the finest grain size and largest volume fraction of secondary phase. Nevertheless, most of the polygonal-shaped Al_2Sm particles that acted as heterogeneous nucleation sites in as-cast alloys were not fragmented during hot deformation. Al_2Sm particles might become the crack source during tensile test, which was one of the reasons for a lower elongation of 3.13%Sm alloy (10 ± 1%).

(v) Textures strengthening. Extruded Mg alloys usually produce a basal texture where the basal plane is parallel to the ED. When the tensile direction is parallel to ED, this kind of texture is unfavorable for the occurrence of basal slip, which gives rise to texture strengthening effect on mechanical properties (Ref 22). However, our results in Fig. 5, 6 and 7 showed that a higher texture intensity did not contribute to a higher strength. For two kinds of typical examples, among the first three alloys which had bimodal grain structures, the 0.32%Sm alloy exhibited the highest texture intensity of 10.703 but the lowest yield strength of 181 ± 2 MPa. Among the latter two alloys which had DRXed fine grains, the 3.13%Sm alloy exhibited a lower texture intensity of 5.647 but a higher yield strength of 198 ± 3 MPa. This is because the texture, grain size and the amount and size distribution of secondary phase change simultaneously. Thus, texture strengthening effect was hard to be separately discussed.

From the above analysis of interacted strengthening factors, it is found that grain refinement, secondary phase distribution and texture are the most important factors determining the mechanical properties of the extruded AZ31−*x*Sm alloys. A better yield strength can be obtained by a smaller DRXed grain size, large amount of $Al_{11}Sm_3$ particles and suitable texture. To obtain this aim, the as-cast alloys may have two features. The first feature lies in the uniform equiaxed grains in the as-cast alloy to exert the microstructure heredity effect. This means Al_2Sm particle is quite necessary due to grain refinement potency, although some large Al_2Sm particle is found to reduce the DRX effect during extrusion. The second feature lies in an enough number of fragmented smaller particles, which can not only act as PSN sites during DRX, but also exhibit secondary phase strengthening effect. Due to the strengthening effects of grain refinement, secondary phase and texture, the as-extruded 3.13% Sm alloy has the optimal strength with YS198MPa, UTS 272 MPa and EL.10%. If the properties are compared with the as-cast values of YS 79 MPa, UTS217MPa and EL.14% (Ref 9), the strength is thought to be greatly improved. Due to the importance of microstructural feature, a schematic diagram showing microstructure evolution of AZ31−*x*Sm alloys under as-cast and as-extruded conditions is drawn in Fig. 8, which would be useful for future development of new low-cost Mg alloys.

4. Conclusions

The microstructures and mechanical properties of extruded AZ31−xSm (x = 0, 0.32, 1.18, 2.17 and 3.13 wt.%) alloys were investigated using OM, SEM–EDS, EBSD and tensile test. The following conclusions can be drawn:

1. With increasing Sm content, the grain size changes in a non-monotonic mode of firstly coarsening and then refining. The first three alloys have bimodal grain structure consisted of unDRXed grains and DRXed grains, while the latter two alloys have fully DRXed fine grains. Such kinds of evolution in grain size and grain structure are closely related to microstructure heredity and quantity of secondary phase particles. Besides a fine grain size in initial alloy, a large amount of $Al_{11}Sm_3$ particles helps DRX due to PSN effect.
2. The texture intensity changes basically in accordance with DRX behavior. However, a typical case is that when big-sized Al_2Sm particle is present, the PSN effect is weakened, which results in an increase in both area fraction of large grains and texture intensity.
3. Grain refinement, secondary phase distribution and texture are the most important factors influencing the mechanical properties of extruded alloys. AZ31 alloy with 3.13% Sm content has the best mechanical property (i.e., YS 198 MPa, UTS 272 MPa and elongation 10%), due to the fine grains, large amount of tiny secondary phase and suitable texture intensity.

Acknowledgments

This work is supported by National Natural Science Foundation of China (Grant No. 51701124). The authors are grateful to Prof. Liming Peng at Shanghai Jiao Tong University (SJTU, China) for access to some experiments and for useful discussion.

References

1. X. Wang, M. Wu, W. Ma, Y. Lu, and S. Yuan, Achieving Superplasticity in AZ31 Magnesium Alloy Processed by Hot Extrusion and Rolling, *J. Mater. Eng. Perform.*, 2016, **25**(1), p 64–67
2. Y. Lou, W. Wu, and L. Li, Inverse Identification of the Dynamic Recrystallization Parameters for AZ31 Magnesium Alloy Using BP Neural Network, *J. Mater. Eng. Perform.*, 2012, **21**(7), p 1133–1140
3. D.H. StJohn, M.A. Easton, Q. Ma, and J.A. Taylor, Grain Refinement of Magnesium Alloys: A Review of Recent Research, Theoretical Developments, and Their Application, *Metall. Mater. Trans. A*, 2013, **44**, p 2935–2949
4. J. Du, J. Yang, M. Kuwabara, W. Li, and J. Peng, Effects of Carbon and/or Alkaline Earth Elements on Grain Refinement and Tensile Strength of AZ31 Alloy, *Mater. Trans.*, 2008, **49**(10), p 2303–2309
5. E. Karakulak and A. Review, Past, Present and Future of Grain Refining of Magnesium Castings, *J. Magnes. Alloys*, 2019, **7**(3), p 355–369
6. D. Qiu, M. Zhang, J.A. Taylor, and P. Kelly, A New Approach to Designing a Grain Refiner for Mg Casting Alloys and Its Use in Mg-Y-Based Alloys, *Acta Mater.*, 2009, **57**(10), p 3052–3059
7. D. Qiu, M.X. Zhang, and P.M. Kelly, Crystallography of Heterogeneous Nucleation of Mg grains on Al_2Y Nucleation Particles in an Mg-10 wt% Y alloy, *Scr. Mater.*, 2009, **61**(3), p 312–315
8. J.C. Dai, M.A. Easton, S.M. Zhu, G.H. Wu, and W.J. Ding, Grain Refinement of Mg-10Gd Alloy by Al Additions, *J. Mater. Res.*, 2012, **27**(21), p 2790–2797
9. M. Sun, X.Y. Hu, L.M. Peng, P.H. Fu, and Y.H. Peng, Effects of Sm on the Grain Refinement, Microstructures and Mechanical Properties of AZ31 Magnesium Alloy, *Mater. Sci. Eng. A*, 2014, **620**, p 89–96
10. X. Hu, P. Fu, D. StJohn, L. Peng, M. Sun, and M. Zhang, On Grain Coarsening and Refining of the Mg-3Al Alloy by Sm, *J. Alloys Compd.*, 2016, **663**, p 387–394
11. C. Wang, J. Dai, W. Liu, L. Zhang, and G. Wu, Effect of Al Additions on Grain Refinement and Mechanical Properties of Mg-Sm Alloys, *J. Alloys Compd.*, 2015, **620**, p 172–179
12. L. Fu, W. Hu, Q. Le, Z. Jia, and L. Lu, The Role of Sm in Precipitates, Grain Sizes, and Tensile Properties of As-Cast and As-Extruded AZ31-0.3La Alloys, *Adv. Eng. Mater.*, 2019, **22**, p 1901215–1901227
13. D. Qiu and M.X. Zhang, The Nucleation Crystallography and Wettability of Mg Grains on Active Al_2Y Inoculants in An Mg-10wt% Y Alloy, *J. Alloys Compd.*, 2014, **586**, p 39–44
14. X. Li, Z. Hu, H. Yan, X. Wu, H. Xie, and Z. Dong, Effect of Sm-Rich Phase on Corrosion Behavior of Hot-Extruded AZ31-1.5Sm Magnesium Alloy, *J. Mater. Eng. Perform.*, 2018, **27**(6), p 3072–3082
15. Z. Hu, R.L. Liu, S.K. Kairy, X. Li, H. Yan, and N. Birbilis, Effect of Sm Additions on the Microstructure and Corrosion Behavior of Magnesium Alloy AZ91, *Corros. Sci.*, 2019, **149**, p 144–152
16. J.D. Robson, D.T. Henry, and B. Davis, Particle Effects on Recrystallization in Magnesium-Manganese Alloys: Particle-Stimulated Nucleation, *Acta Mater.*, 2009, **57**(9), p 2739–2747
17. T. Laser, Ch Hartig, M.R. Nürnberg, D. Letzig, and R. Bormann, The Influence of Calcium and Cerium Mischmetal on the Microstructural Evolution of Mg-3Al-1Zn during Extrusion and Resulting Mechanical Properties, *Acta Mater.*, 2008, **56**(12), p 2791–2798
18. X.Y. Xu, Y.F. Wang, H.Y. Wang, T. Wang, and Q.C. Jiang, Influences of Pre-existing $Mg_{17}Al_{12}$ Particles on Static Recrystallization Behavior of Mg-Al-Zn Alloys at Different Annealing Temperatures, *J. Alloys Compd.*, 2019, **787**, p 1104–1109
19. H.E. Friedrich and B.L. Mordike, *Magnesium Technology: Metallurgy, Design Data, Applications*, Springer, Berlin, Heidelberg, 2006
20. S.H. Kim, B.S. You, and S.H. Park, Effect of Billet Diameter on Hot Extrusion Behavior of Mg-Al-Zn Alloys and Its Influence on Microstructure and Mechanical Properties, *J. Alloys Compd.*, 2017, **690**, p 417–423
21. N. Petch, The Cleavage Strength of Polycrystals, *J. Iron Steel Inst.*, 1953, **174**, p 25–28
22. H. Huang, G.Y. Yuan, Z.H. Chu, and W.J. Ding, Microstructure and Mechanical Properties of Double Continuously Extruded Mg-Zn-Gd-Based Magnesium Alloys, *Mater. Sci. Eng. A*, 2013, **560**, p 241–248